459

Experimental behaviours of steel tube confined concrete (STCC) columns

Lin-Hai Han†

*Department of Civil Engineering, Tsinghua University, Beijing, 100084,
P. R. China*

Guo-Huang Yao‡ and Zhi-Bo Chen‡†

*College of Civil Engineering and Architecture, Fuzhou University, Gongye Road 523,
Fuzhou, Fujian Province, 350002, P. R. China*

Qing Yu‡‡

*Institute of International Engineering Project Management,
Tsinghua University, Beijing, 100084, P. R. China*

Abstract.   In recent years, the use of steel tube confined concrete (STCC) columns has been the interests of many structural engineers. The present study is an attempt to study the monotonic and cyclic behaviours of STCC columns. For the monotonic behaviours, a series of tests on STCC stub columns (twenty one), and beam-columns (twenty) were carried out. The main parameters varied in the tests are: (1) column section types, circular and square; (2) tube diameter (or width) to thickness ratio, from 40 to 162, and (3) load eccentricity ratio (e/r), from 0 to 0.5. For the cyclic behaviours, the test parameters included the sectional types and the axial load level (n). Twelve STCC column specimens, including 6 specimens with circular sections and 6 specimens with square sections were tested under constant axial load and cyclically increasing flexural loading. Comparisons are made with predicted column strengths and flexural stiffness using the existing codes. It was found that STCC columns exhibit very high levels of energy dissipation and ductility, particularly when subjected to high axial loads. Generally, the energy dissipation ability of the columns with circular sections was much higher than those of the specimens with square sections. Comparisons are made with predicted column strengths and flexural stiffness using the existing codes such as AIJ-1997, AISC-LRFD-1994, BS5400-1979 and EC4-1994.

Key words: composite columns; confined concrete; beam columns; design; concrete; hollow sections; seismic design; cyclic load; flexural stiffness; ductility

---

†Professor, Corresponding author, E-mail: lhhan@mail.tsinghua.edu.cn
‡Ph.D. Student
‡†Master Student
‡‡Associate Professor

1. Introduction

Concrete filled steel tubular (CFST) columns have several structural and constructional benefits, such as high strength and fire resistance, large stiffness and ductility, omission of formwork and thus reduce the construction cost and time (ASCCS 1997, Schneider 1998, Schneider *et al.* 2004). These advantages have been recognized and have led to the increased use of concrete-filled HSS columns in some of the recent tall buildings in China (Han *et al.* 2003b).

It is well known that, for CFST columns, when the steel tube and the concrete core were both loaded, the steel tube carried some direct axial load, but the concrete carried less axial load than if only the concrete core was loaded, because the steel tube (which was axially loaded in this case) was less effective in confining the concrete core than if it was not axially loaded. Therefore, if the confinement of the column section and the ductility of the member are among the most important design factors, then it is recommended only the concrete core be loaded. Fig. 1 illustrates a schematic view of steel tube confined concrete (STCC) columns.

It is expected that, steel tube confined concrete (STCC) columns offer several advantages over ordinary CFST columns (Aboutaha and Machado 1998), i.e.,

(1) Smaller longitudinal axial loads are transferred through the steel tube, and thus maximize the effectiveness of the steel tube in confining the concrete core.

(2) The beam-column joint of the STCC column system is a well detailed ordinary reinforced concrete (RC) beam–column joint.

(3) The possibility of buckling of the steel tube is virtually reduced due to the steel tube in STCC columns carries very small axial compressive loads.

In the past, both bonded and unbonded specimens for concrete-filled steel tubes subjected to concentric axial compression had been tested, including application of the axial load to the composite steel-concrete section and to the concrete core only, such as Fam *et al.* (2004), Johansson (2002), Orito *et al.* (1987), O'Shea and Bridge (1997a, 1997b) and Sakino *et al.* (1985). It was found that, in general, the axial strengths of the unbonded short columns were slightly increased, compared to those of the bonded ones, while the stiffness of the unbonded specimens was slightly reduced.
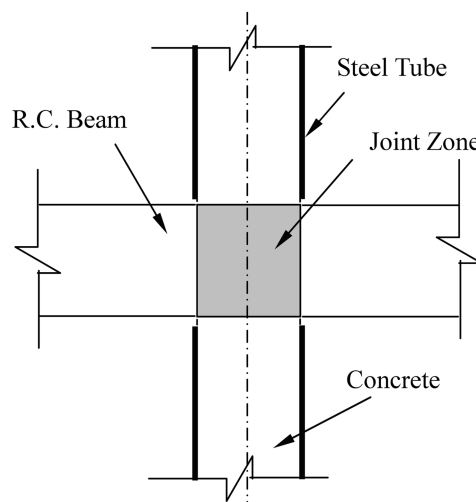
Fig. 1 A schematic view of the STCC column

Fam *et al.* (2004) also present an experimental work and analytical modeling for concrete-filled steel tubes subjected to combined axial compression and lateral cyclic loading. Both bonded and unbonded specimens were tested. The research indicates that the bond and end loading conditions did not influence the flexural strength of beam-column members significantly. However, the axial strengths of the unbonded short columns were slightly increased, compared to those of the bonded ones, while the stiffness of the unbonded specimens was slightly reduced.

The behavior of STCC columns under both monotonic and cyclic loading has been experimentally investigated and the results presented in this paper. The differences of this test program compared with the similar studies carried out by other researchers mentioned above are as followings:

(1) Both STCC columns with circular sections and with square sections were tested, seldom STCC columns with square sections were reported before.

(2) Both STCC columns and beam columns were tested.

(3) Axial load level (*n*) range is wide for the cyclic tests, *n* ranges from 0 to 0.74.

The lack of information on STCC columns with square sections, as well as the behaviours of STCC beam columns under both monotonic and cyclic loadings, indicates a need for further research in this area.

The aims of this paper were thus fourfold: first, to report a series of monotonic and cyclic tests on STCC columns. Second, to analyze influence of several parameters on the behaviours of STCC stub columns and beam columns. Third, to analyze influence of several parameters on the behaviours of moment versus curvature response, and lateral load versus lateral deflection relationship for the composite columns. And finally, to compare the predicted column strengths and flexural stiffness using the existing codes.

2 Material properties and specimen preparations

2.1. Material properties

Strips of the steel tubes were tested in tension. Three coupons were taken from each face of the steel tube, from these tests, the average yield strength (f_{sy}) and the modulus of elasticity of the steel tubes were found to be 307 MPa and 204800 MPa respectively.

A kind of self-consolidating concrete (SCC) or self-compacting concrete mix was designed for compressive cube strength (f_{cu}) at 28 days of approximately 39 MPa. The modulus of elasticity (E_c) of concrete was measured, the average value being 33010 MPa. The mix proportions were as follows:

- Cement: 300 kg/m^3
- Blast furnace slag: 200 kg/m^3
- Water: 181 kg/m^3
- Sand: 994 kg/m^3
- Coarse aggregate: 720 kg/m^3
- Additional high-range water reducer (HRWR): 5.2 kg/m^3

A typical test set up (L-Box) can be used to simulate the casting process by forcing an SCC sample to flow through obstacles under a static pressure (Han and Yao 2004). The flow time from the sliding door to the front door of the L-box, the flow speed, and the flow distance of the SCC were recorded. The fresh properties of the SCC mixture were as follows:

- Slump flow (mm): 270
- Fresh air content (%): 4.5

- Unit weight (kg/m^3): 2350
- Flow time (sec): 13
- Flow speed (mm/sec): 61.5
- Flow distance (mm): 1110

In all the concrete mixes, the fine aggregate used was silica-based sand, the coarse aggregate was carbonate stone from Fuzhou City, South of China.

The average cube strength at the time of test was 42.6 MPa.

2.2. Specimen preparations

In order to achieve the desired the tube diameter (or width) to thickness ratio(D/t), the steel tubes were all manufactured from mild steel sheet, with plates were cut from the sheet, tack welded into a circular or square shape and then welded with a single bevel butt weld. The ends of the steel tube sections were cut and machined to required length. The insides of the tubes were wire brushed to remove any rust and loose debris. The SCC was filled in layers without any vibrations. The specimens were placed upright to air-dry until heating.

For CFST columns, two end plates were welded with the steel tubes. For STCC columns, both the top and the bottom ends of the columns were reinforced by steel bars, to ensure the ends do not fail during the tests. Two end plates were welded with the steel bars.

Table 1 Specimen labels and sectional capacities (stub columns)

Section types	No.	Specimen	$D \times t$ (mm)	L(mm)	D/t	N_{ue} (kN)		SI (%)
						Measured value	Average value	
Circular	1	SC1-1	60 × 1.48	180	40.5	220	217.5	-2
	2	SC1-2	60 × 1.48	180	40.5	215		
	3	SCCFT1	60 × 1.48	180	40.5	222	222	100
	4	SC2-1	120 × 1.48	360	81.1	610	635	9.1
	5	SC2-2	120 × 1.48	360	81.1	660		
	6	SCCFT2	120 × 1.48	360	81.1	582	582	100
	7	SC3-1	180 × 1.48	540	121.6	1311	1295.5	12.1
	8	SC3-2	180 × 1.48	540	121.6	1280		
	9	SCCFT3	180 × 1.48	540	121.6	1155	1155	100
	10	SC4-1	240 × 1.48	720	162.2	2300	2225	16.3
	11	SC4-2	240 × 1.48	720	162.2	2150		
	12	SCCFT4	240 × 1.48	720	162.2	1912	1912	100
Square	1	SS1	60 × 1.48	180	40.5	228	228	-1.7
	2	SSCFT1	60 × 1.48	180	40.5	232	232	100
	3	SS2	120 × 1.48	360	81.1	700	700	10.8
	4	SSCFT2	120 × 1.48	360	81.1	632	632	100
	5	SS3	180 × 1.48	540	121.6	1400	1400	13.4
	6	SSCFT3	180 × 1.48	540	121.6	1235	1235	100
	7	SS4-1	240 × 1.48	720	162.2	2280	2290	13.6
	8	SS4-2	240 × 1.48	720	162.2	2300		
	9	SSCFT4	240 × 1.48	720	162.2	2016	2016	100

3. Stub column and eccentrically loaded column test

The experimental study was not only to determine the maximum load capacity of the specimens, but also to investigate the failure pattern up to and beyond the ultimate load. The experimental program consisted of two stages, which are described below and designated as types I and II.

3.1. Type I: stub column tests

A total of twenty one stub specimens were tested. A summary of the specimens is presented in Table 1. The lengths of the stub columns (L) were chosen to be three times the diameter (for CHS) or the width (for SHS) to avoid the effects of overall buckling and end conditions (Han *et al.* 2001).

All the tests were performed on a 5000 kN capacity testing machine. The specimens were placed into the testing machine and the loads were applied on the specimens directly. Fig. 2 gives a schematic view of the test arrangement. The loading ram is a solid steel plate, which acts like an end stiffener. Eight strain gauges were used for each specimen to measure strains at the middle height. Two linear voltage displacement transducers (LVDTs) were used to measure the axial deformation, shown as in Fig. 2. A load interval of less than one tenth of the estimated load capacity was used. Each load interval was maintained for about 2 to 3 minutes.

It was found that some features of the STCC and CFST specimens were different. For the CFST, local buckling effects become increasingly important because the larger longitudinal axial loads are transferred through the steel tube, local buckling of the steel tube occurred earlier and more obviously than STCC specimens. The change in buckling mode of the steel tube had somewhat effect on the ultimate strength of the specimen. Typical failure modes of the stub columns with different sections were shown in Fig. 3.

Total of the tested curves of load (N) versus axial strain (ε) is shown in Fig. 4 and Fig. 5 for specimens with circular and square sections respectively. All of the tested curves of load (N) versus lateral strain (ε) are shown in Fig. 6 and Fig. 7 for specimens with circular and square sections respectively. The maximum loads (N_{ue}) obtained in the test are summarised in Table 1.

(a) STCC columns (b) CFST columns
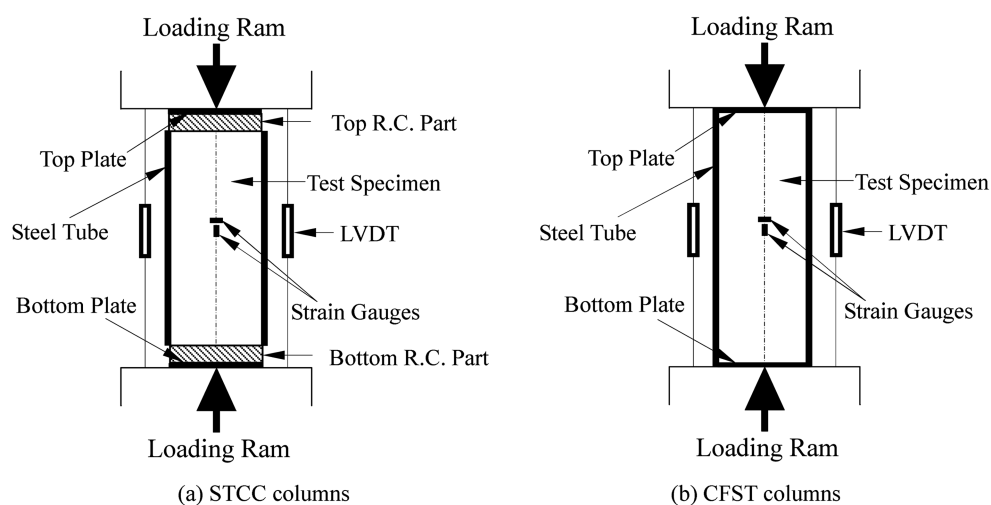
Fig. 2 Arrangement of stub column tests
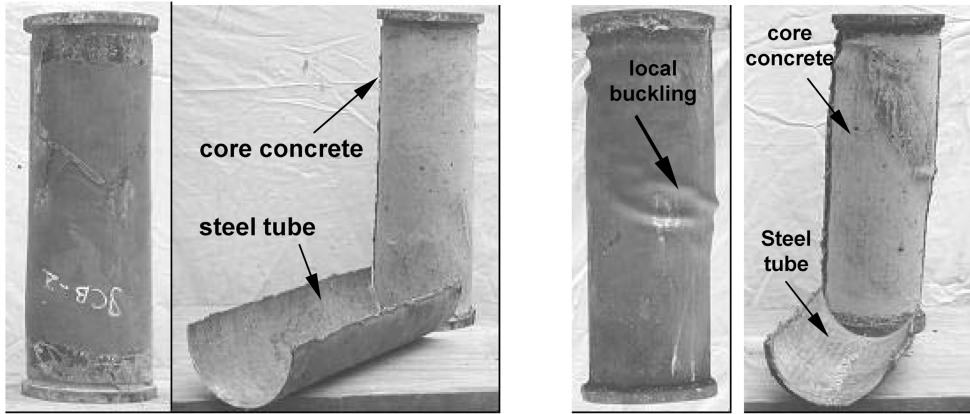
(a) STCC   (b) CFST

(1) Circular sections
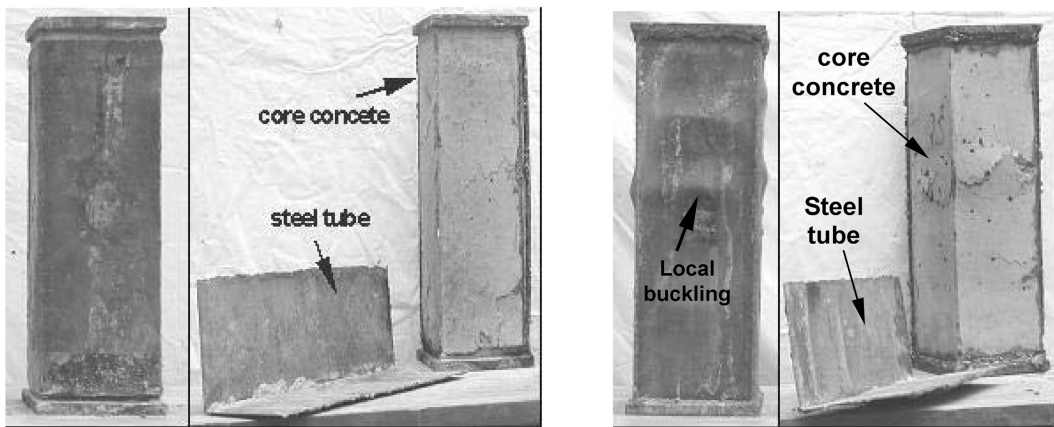
(a) STCC   (b) CFST

(2) Square sections

Fig. 3 Stub column failure mode
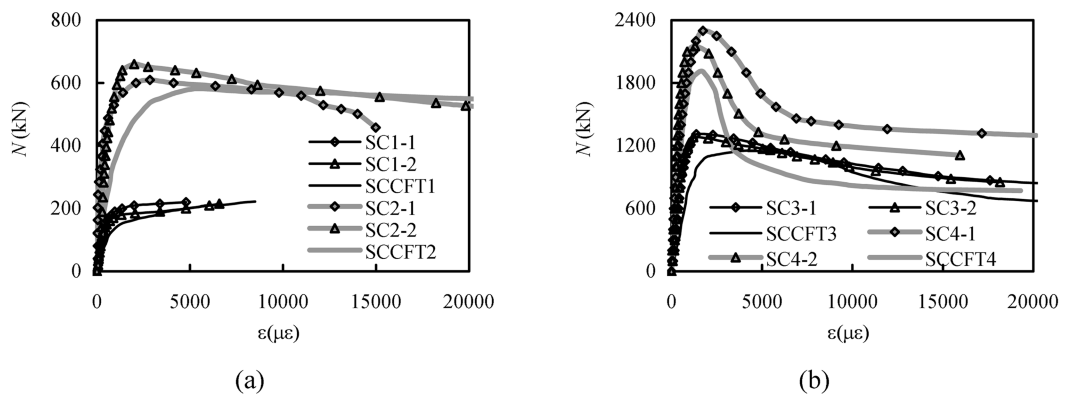
(a)   (b)

Fig. 4 Axial load (N) versus axial strain (ε) curves (circular sections)
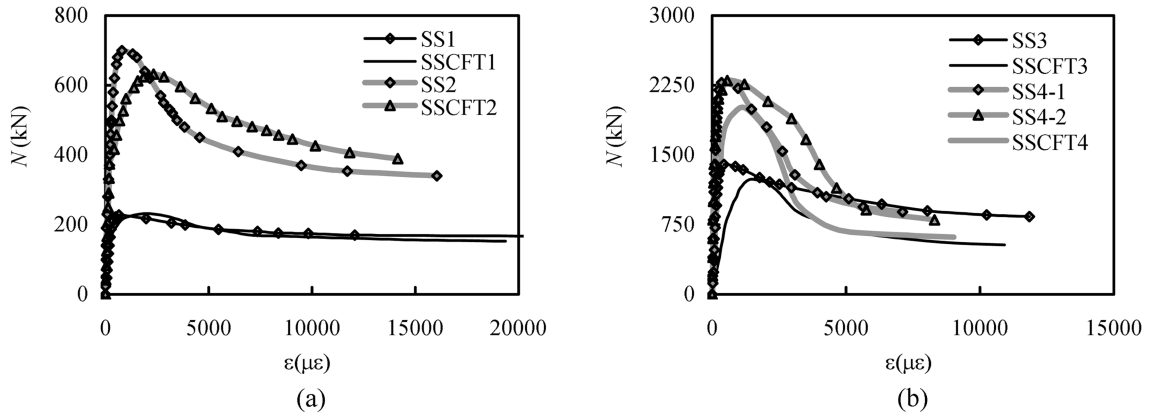
Fig. 5 Axial load (*N*) versus axial strain (*ε*) curves (square sections)
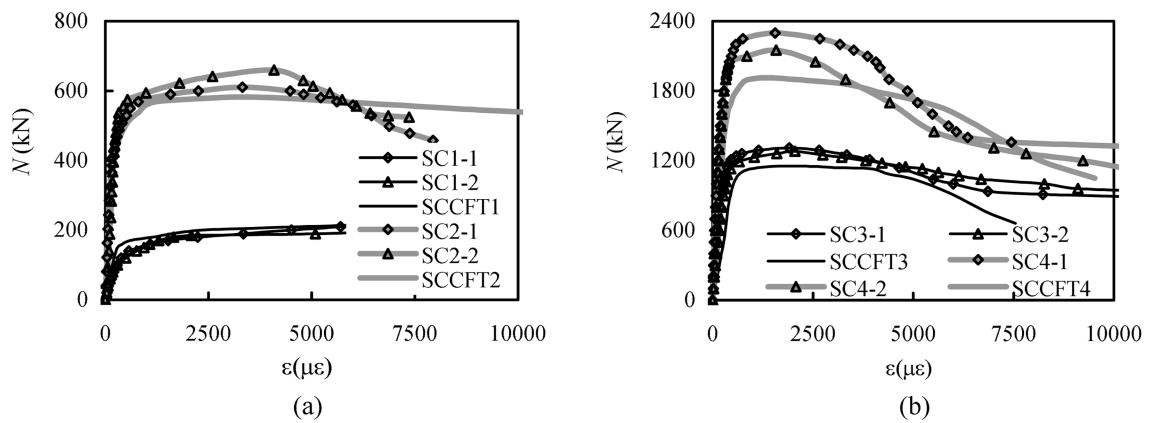
Fig. 6 Axial load (*N*) versus lateral strain (*ε*) curves (circular sections)
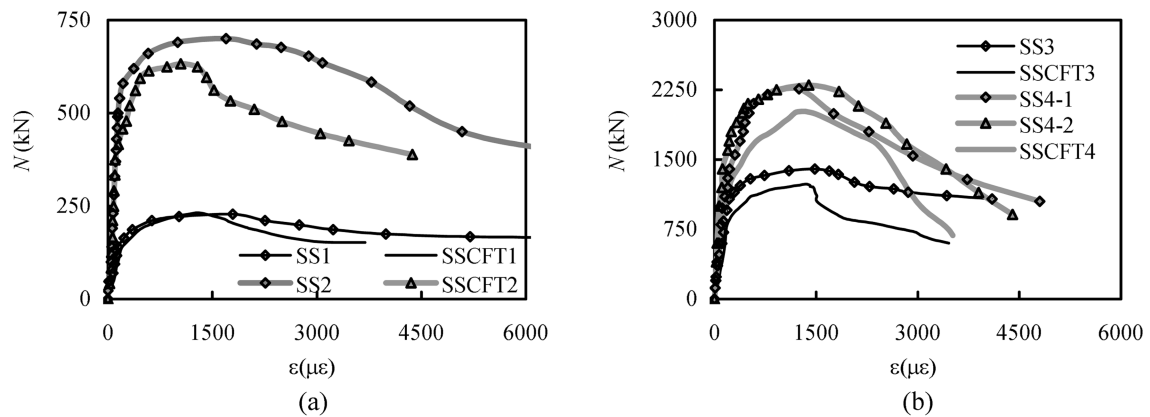
Fig. 7 Axial load (*N*) versus lateral strain (*ε*) curves (square sections)

3.2. Type II: eccentrically loaded column test

Twenty tests on concentrically or eccentrically loaded composite columns and beam-columns were carried out. A summary of the specimens is presented in Table 2 where the section sizes, slenderness ratios (λ) and load eccentricities ratio (e/r) are given.

The desired eccentricity was achieved by accurately machining grooves 6 mm deep into the stiff end plate that was welded together with the steel tubes (for CFST) or reinforced bars similar to that of STCC stub column specimens (for STCC). For the pure axial compression column, the groove was in the middle of the plate. The endplate was very stiff with a thickness of 30 mm. The axial load was applied through a very stiff top platen with an offset triangle hinge, which also allowed specimen rotation to simulate pin-ended supports. Both the endplate and the top platen were made of very hard and very high strength steel. Eight strain gauges were used for each specimen to measure the longitudinal and transverse strains at the middle height. Two displacement transducers were used to measure the axial deformation. Three linear voltage displacement transducers (LVDTs) were used to measure the lateral deflection.

A load interval of less than one tenth of the estimated load capacity was used. Each load interval was maintained for about 2 to 3 minutes. At each load increment the strain readings and the deflection measurements were recorded. All specimens were loaded to failure. Each test took approximately 35 minutes to reach the maximum load and 90 minutes to complete.

Table 2 Specimen labels and member capacities (long columns)

Section type	No.	Specimen	$D \times t$ (mm)	L (mm)	λ	e (mm)	e/r	N_{ue} (kN) Measured value	N_{ue} (kN) Average value	SI (%)
Circular	1	LCA-1	120 × 1.48	750	25	0	0	548	---	---
	2	LCA-2	120 × 1.48	750	25	0	0	556		
	3	LCB-1	120 × 1.48	1500	50	0	0	468	467	-8.4
	4	LCB-2	120 × 1.48	1500	50	0	0	466		
	5	LCCFT-1	120 × 1.48	1500	50	0	0	510	510	100
	6	LCC-1	120 × 1.48	1500	50	15	0.25	324	---	---
	7	LCC-2	120 × 1.48	1500	50	15	0.25	318		
	8	LCD-1	120 × 1.48	1500	50	30	0.5	216	217	-21.9
	9	LCD-2	120 × 1.48	1500	50	30	0.5	218		
	10	LCCFT-2	120 × 1.48	1500	50	30	0.5	278	278	100
Square	1	LSA-1	120 × 1.48	750	21.6	0	0	642	---	---
	2	LSA-2	120 × 1.48	750	21.6	0	0	638		
	3	LSB-1	120 × 1.48	1500	43.3	0	0	602	608	-8.6
	4	LSB-2	120 × 1.48	1500	43.3	0	0	614		
	5	LSCFT-1	120 × 1.48	1500	43.3	0	0	665	665	100
	6	LSC-1	120 × 1.48	1500	43.3	15	0.25	456	---	---
	7	LSC-2	120 × 1.48	1500	43.3	15	0.25	430		
	8	LSD-1	120 × 1.48	1500	43.3	30	0.5	324	324.5	-8.8
	9	LSD-2	120 × 1.48	1500	43.3	30	0.5	325		
	10	LSCFT-2	120 × 1.48	1500	43.3	30	0.5	356	356	100

Typical failure mode was overall buckling failure. When the load was small, the lateral deflection at middle height is small and approximately proportional to the applied load. When the load reached about 60% to 70% of the maximum load, the lateral deflection at middle height started to increase significantly. It was found that the features of the STCC and CFST specimens were very similar.

Fig. 8 gives a general view of the beam-column specimens after tests.

The load (N) versus deflection (u_m) curves for the specimens with circular and square sections are presented in Fig. 9, where, u_m is the deflection at mid-height of the beam-column. The maximum loads (N_{ue}) obtained in the test are summarised in Table 2.

(a) Circular sections　　　(b) Square sections
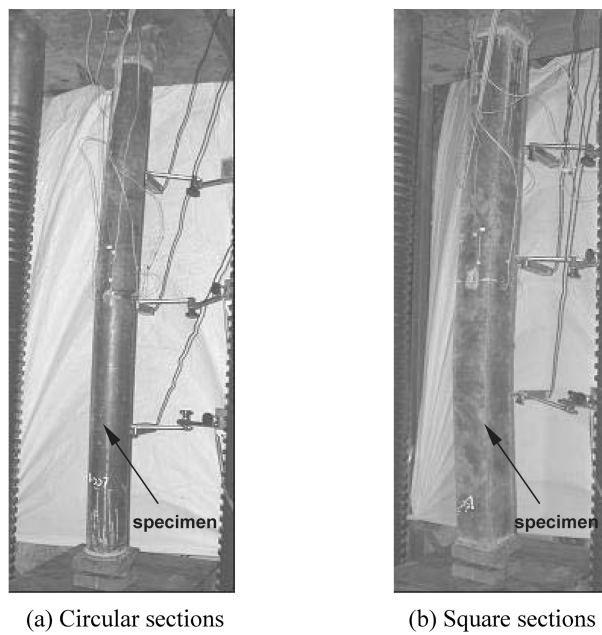
Fig. 8 Long column failure mode

(a) Circular specimens　　　(b) Square specimens
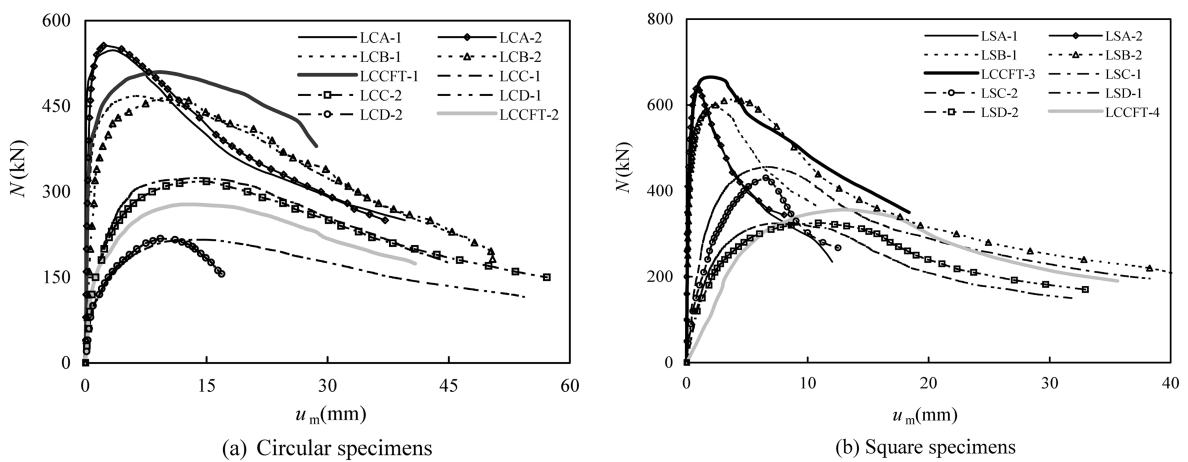
Fig. 9 Axial load versus lateral deflection at mid-height of test specimens

(a) Circular specimens   (b) Square specimens
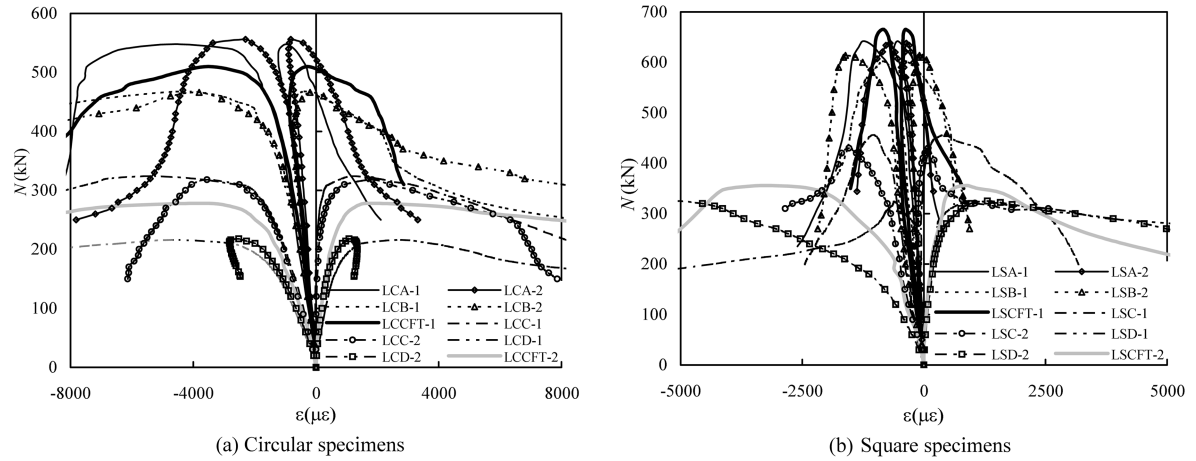
Fig. 10 Axial load versus extreme fiber strains at mid-height of test specimens

The axial load (N) versus extreme fiber compressive and tensile strains for the specimens with circular and square sections are shown in Fig. 10.

It was found that all the test specimens behaved in a relatively ductile manner and testing proceeded in a smooth and controlled way.

3.3. Analysis of test results and discussions

3.3.1 Strength index

For convenience of comparisons of the ultimate strength of the composite columns, the strength index (SI) is defined as following:

$$SI = \frac{N_{ueSTCC} - N_{ueCFST}}{N_{ueCFST}} \tag{1}$$

where N_{ueSTCC} and N_{ueCFST} are the loading capacities of the STCC and CFST specimens respectively.

The strength index (SI) so determined is listed in Table 1 and in Table 2 for the stub columns and eccentrically loaded columns respectively, in the calculations, N_{ueSTCC} is taken as the average value of member capacities of the tested specimens.

It can be found from Table 1 that, generally, the section capacities of the STCC specimens are lightly higher than those of the CFST specimens.

The test results summarised in Table 2 clearly show that, generally, the ultimate strengths (N_{ue}) of the CFST members were 8.4% to 21.9% higher than those of the STCC columns.

3.3.2. Comparisons of bearing capacity of the composite columns

The bearing capacities predicted of the STCC columns using the following four design methods for CFST are compared with the column test results those obtained in the current tests:

- AIJ (1997)

- AISC-LRFD (1999)
- BS5400 (1979)
- EC4 (1994)

In all design calculations, the material partial safety factors were set to unity.

Predicted bearing capacities (N_{uc}) using the different methods are compared with test results (N_{ue}) in Table 3 and Table 4 for specimens with circular and square sections respectively.

Results in Table 3 show that both AIJ, AISC-LRFD and BS5400 are conservative for predicting the strengths of the specimens with circular sections. Overall, AISC-LRFD gave a member capacity about 22% lower than the results obtained in the tests. AIJ gave a member capacity about 10% lower than these of the measured ultimate strength. EC4 gave a member capacity about 3% higher than these of the measured ultimate strength. Overall, the proposed method by BS5400 give a mean of 0.968, and a COV of 0.090, is the best predictor to predict the ultimate strength of the STCC columns.

Results in Table 4 clearly show that both AIJ, AISC-LRFD, and BS5400 are conservative for predicting the strengths of the STCC specimens with square sections. Overall, AISC-LRFD and BS5400 gave a bearing capacity about 13% to 15% lower than the results obtained in the tests. AIJ gave a member capacity about 5% lower than these of the measured ultimate strength. However, EC4 gave a member capacity about 6% higher than these of the measured ultimate strength, gave an unsafe prediction. Overall, the proposed method by AIJ gave a mean of 0.954 and a COV of 0.053 respectively, and it is the best predictor to predict the ultimate strength of the STCC columns with square sections.

Table 3 Comparison between predicted column capacities and test results (circular columns)

No.	Specimen	N_{ue} (kN)	AISC-LRFD (1999)		AIJ (1997)		BS5400 (1979)		EC4 (1994)	
			N_{uc} (kN)	$\dfrac{N_{uc}}{N_{ue}}$	N_{uc} (kN)	$\dfrac{N_{uc}}{N_{ue}}$	N_{uc} (kN)	$\dfrac{N_{uc}}{N_{ue}}$	N_{uc} (kN)	$\dfrac{N_{uc}}{N_{ue}}$
1	SC1-1	220	158	0.718	182	0.827	238	1.082	211	0.959
2	SC1-2	215	158	0.735	182	0.847	238	1.107	211	0.981
3	SC2-1	610	487	0.798	534	0.875	649	1.064	659	1.080
4	SC2-2	660	487	0.738	534	0.809	649	0.983	659	0.998
5	SC3-1	1311	983	0.750	1053	0.803	1223	0.933	1308	0.998
6	SC3-2	1280	983	0.768	1053	0.823	1223	0.955	1308	1.022
7	SC4-1	2300	1647	0.716	1739	0.756	1985	0.863	2155	0.937
8	SC4-2	2150	1647	0.766	1739	0.809	1985	0.923	2155	1.002
9	LCA-1	548	474	0.865	516	0.942	579	1.057	556	1.015
10	LCA-2	556	474	0.853	516	0.928	579	1.041	556	1.000
11	LCB-1	468	435	0.929	453	0.968	476	1.017	490	1.047
12	LCB-2	466	435	0.933	453	0.972	476	1.021	490	1.052
13	LCC-1	324	228	0.704	301	0.929	272	0.840	343	1.059
14	LCC-2	318	228	0.717	301	0.947	272	0.855	343	1.079
15	LCD-1	216	154	0.713	235	1.088	190	0.880	245	1.134
16	LCD-2	218	154	0.706	235	1.078	190	0.872	245	1.124
Mean value			0.776		0.900		0.968		1.030	
COV(Coefficient of Variation)			0.078		0.098		0.090		0.055	

Table 4 Comparison between predicted column capacities and test results (square columns)

No.	Specimen	N_{ue} (kN)	AISC-LRFD (1999)		AIJ (1997)		BS5400 (1979)		EC4 (1994)	
			N_{uc} (kN)	$\dfrac{N_{uc}}{N_{ue}}$	N_{uc} (kN)	$\dfrac{N_{uc}}{N_{ue}}$	N_{uc} (kN)	$\dfrac{N_{uc}}{N_{ue}}$	N_{uc} (kN)	$\dfrac{N_{uc}}{N_{ue}}$
1	SS1	228	202	0.886	203	0.890	200	0.877	220	0.965
2	SS2	700	620	0.886	621	0.887	609	0.870	693	0.990
3	SS3	1400	1252	0.894	1253	0.895	1224	0.874	1417	1.012
4	SS4-1	2280	2097	0.920	2098	0.920	2047	0.898	2391	1.049
5	SS4-2	2300	2097	0.912	2098	0.912	2047	0.900	2391	1.039
6	LSA-1	642	608	0.947	617	0.961	597	0.930	686	1.069
7	LSA-2	638	608	0.953	617	0.967	597	0.936	686	1.075
8	LSB-1	602	570	0.947	596	0.990	562	0.934	642	1.066
9	LSB-2	614	570	0.928	596	0.971	562	0.915	642	1.046
10	LSC-1	456	318	0.697	421	0.923	355	0.779	490	1.075
11	LSC-2	430	318	0.740	421	0.979	355	0.826	490	1.140
12	LSD-1	324	220	0.679	339	1.046	259	0.799	361	1.114
13	LSD-2	325	220	0.677	339	1.043	259	0.797	361	1.111
Mean value			0.853		0.954		0.873		1.059	
COV (Coefficient of Variation)			0.110		0.053		0.056		0.049	

3.3.3. Strength ratio

The strength ratio (SR) as following is defined to quantify the section strength of the STCC stub columns, i.e.,

$$SR = \frac{N_{ue}}{A_c \cdot f_c'} \tag{2}$$

where, f_c' is concrete cylinder strength.

The strength ratio (SR) against D/t is shown in Fig. 11(a) and Fig. 11(b) for the specimens with circular and square sections respectively. It can be found that, in general, SR decreases with the increase of D/t. The reason is that the constraining effect between the steel tube and the concrete core for the specimens decreases with the increase of D/t, i.e., the composite action between steel tube and core concrete becomes smaller.

It can also be found that generally, the values of SR for circular sections are higher than that of the square specimens with the same D/t. The reason is expected that the constraining effect between the steel tube and the concrete core for the circular specimens is higher than that of the square specimens.

3.3.4. Axial strain and lateral strain

The axial strain corresponding to the ultimate load (ε_{Amax}) against D/t for the tested specimens is shown in Fig. 12. It can be seen from Fig. 12 that generally, the values of ε_{Amax} for STCC columns are smaller than that of the CFST columns under the same D/t. It was found that, for circular sections, ε_{Amax} ranges from 1200 to 2855 $\mu\varepsilon$, and 1693 to 5454 $\mu\varepsilon$ for STCC and CFST columns respectively. For square sections, ε_{Amax} ranges from 320 to 799 $\mu\varepsilon$, and 524 to 2326 $\mu\varepsilon$ for STCC and CFST columns

(a) Circular sections   (b) Square sections
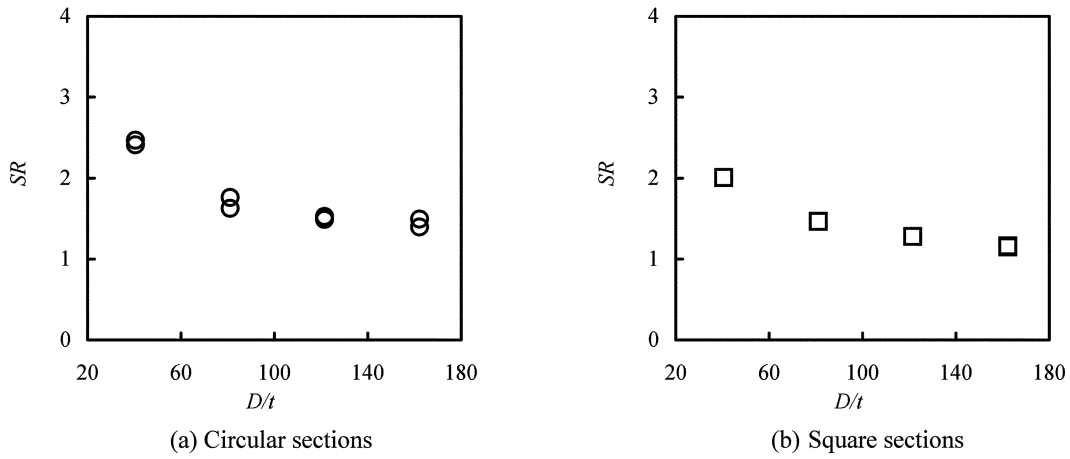
Fig. 11 SR [$= N_{ue} / (A \cdot f_c')$] versus D/t relations

(a) Circular sections   (b) Square sections
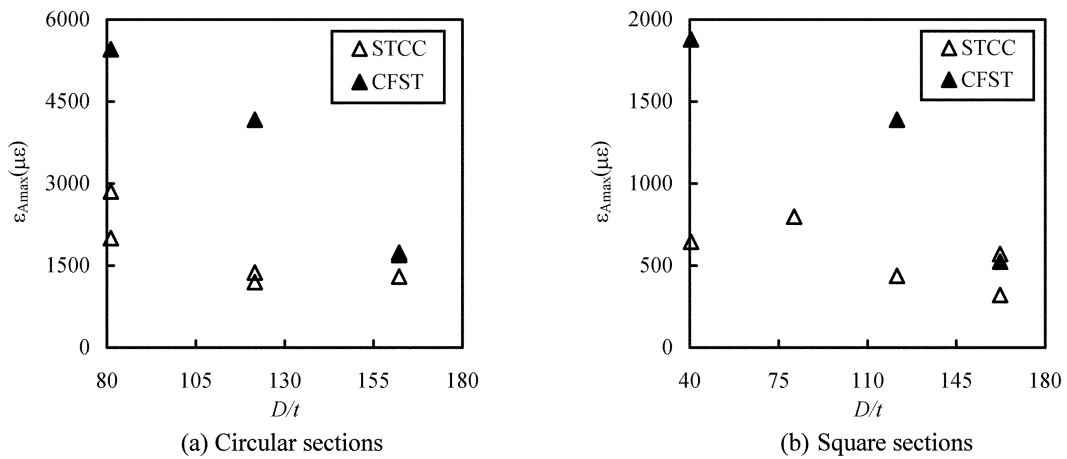
Fig. 12 Axial strain (ε_{Amax}) versus D/t relations

respectively.

The lateral strain corresponding to the ultimate load (ε_{Lmax}) against D/t for the tested specimens is shown in Fig. 13. It can be seen from Fig. 13 that generally, the values of ε_{Lmax} for STCC columns are bigger than those of the CFST columns with the same D/t. It was found that, for circular sections, ε_{Lmax} ranges from 1555 to 4090 $\mu\varepsilon$, and 1375 to 3497 $\mu\varepsilon$ for STCC and CFST columns respectively. For square sections, ε_{Lmax} ranges from 1250 to 1795 $\mu\varepsilon$, and 1046 to 1369 $\mu\varepsilon$ for STCC and CFST columns respectively.

The reasons are that, for CFST columns, the steel tube and the concrete core were both loaded, the steel tube carried some direct axial load, the steel tube was less effective in confining the concrete core than if it was not axially loaded, and thus lead to bigger ε_{Amax} than those the STCC columns. In additional, due to steel tubes in STCC columns can provide more effective confinement to the concrete core than those of the CFST columns, and thus lead to bigger ε_{Lmax}.

(a) Circular sections   (b) Square sections
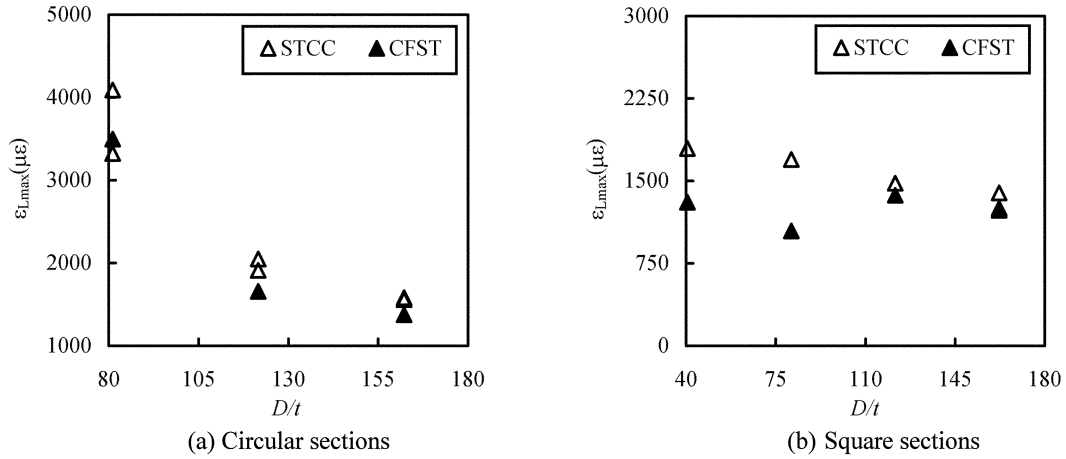
Fig. 13 Lateral strain (ε_{Lmax}) versus D/t relations

4. Cyclically loaded beam column test

4.1. Specimen preparation

Twelve STCC column specimens, including 6 specimens with circular sections and 6 specimens with square sections were tested. The test parameters included the sectional types and the axial load level (n). The axial load level (n) in this paper is defined as following, i.e.,

$$n = \frac{N_o}{N_u} \tag{3}$$

Where N_0 is the axial load applied on the composite specimens; N_u is the axially compressive capacity of the STCC columns, and can be estimated by using the mechanics model described in Han *et al.* (2001, 2004) for CFST columns. Concrete strength at the time of test was used in the calculations.

The details of each column are listed in Table 5, where t is thickness of the steel tube. The tube diameter and the width to thickness ratio (D/t) of the specimens with circular and square sections listed in Table 5 are 81.

4.2. Cyclic test apparatus

The specimens were tested under combined constant axial load and cyclically increasing flexural load. The test length of the specimens is 1500 mm.

Similar test setup with CFST beam-column specimens, which was described in detail by Han *et al.* (2003a), Han and Yang (2005) was used in this study. The ends of the specimens were attached to cylindrical bearings and were free to rotate in-plane, and thus simulating pin-pin end conditions. The axial load (N_o) was applied and maintained constant by a 1000 kN hydraulic ram. A hydraulic pump was used to control the axial load. Precautions were made to avoid any eccentricity in the axial load application by very careful alignment of the test setup. The flexural loading was applied by imposing cyclically lateral loading in the middle of the specimen. The specimen was confined in the middle part

Table 5 Summary of cyclic test information

Section type	No.	Specimen Number	$D \times t$ (mm)	N_o (kN)	n	P_{ue} (kN)	K_{ie} (kN.m^2)	K_{se} (kN.m^2)	Dissipated energy (m.kN)
Circular	1	CCA-1	120×1.48	0	0	24.68	358	343	14.57
	2	CCA-2	120×1.48	0	0	24.55	340	300	13.31
	3	CCB-1	120×1.48	164	0.37	30.1	378	360	16.87
	4	CCB-2	120×1.48	164	0.37	29.15	370	349	16.28
	5	CCC-1	120×1.48	328	0.74	22.85	363	332	6.91
	6	CCC-2	120×1.48	328	0.74	23.2	365	307	8.03
Square	1	CSA-1	120×1.48	0	0	33.99	509	422	14.22
	2	CSA-2	120×1.48	0	0	33.55	644	497	12.54
	3	CSB-1	120×1.48	193	0.34	39.98	534	464	6.25
	4	CSB-2	120×1.48	193	0.34	40.05	511	472	10.88
	5	CSC-1	120×1.48	387	0.68	31.18	562	476	2.44
	6	CSC-2	120×1.48	387	0.68	30.78	514	438	2.73

by a very rigid stub made of high strength steel. The stub was designed and was made of two separate halves of a box with a concentric hole that exactly fit the specimen. The two halves were pushed against the specimen and connected together using eight high strength bolts. The stub may provide effective confinement along the middle 180 mm of the specimens with circular sections, and 150 mm of the specimens with square sections respectively. The stub was attached with a MTS hydraulic ram having 250 kN capacity. Both strain gauges and string pots were used to measure the bending curvature. The in-plane displacements were measured as locations along the specimen test-length by displacement transducers.

The lateral loading history was generally based on ATC-24 (1992) guidelines for cyclic testing of structural steel components. The loading history included elastic cycles and inelastic cycles. The elastic cycles were conducted under load control at load levels of 0.25 P_u, 0.5 P_u and 0.7 P_u, where P_u was the estimated lateral load capacity, which was estimated as the moment capacity (M_u) predicted by using the method presented by EC4 (1994) for CFST columns divided by one quarter of the testing length (1.5 m). Two cycles were imposed at each of the lateral load levels of 0.25, 0.5 and 0.7 P_u. The secant stiffness (K_{sec}) of the specimen during the first 0.7 P_u cycle was used to determine the yield level lateral displacement ($\Delta_y = 0.7 \ P_u/K_{sec}$). The inelastic cycles were then taken to lateral displacement levels of Δ_y, $1.5\Delta_y$, $2\Delta_y$, $3\Delta_y$, $5\Delta_y$, $7\Delta_y$, $8\Delta_y$ and etc. Three cycles were imposed at each displacement levels of Δ_y, $1.5\Delta_y$ and $2\Delta_y$, two cycles were imposed at each additional displacement levels described above. No displacements at the reaction blocks were found until the beam-column specimens bowed after reaching the failure load.

4.3. Experimental results and specimen behavior

All of the test specimens behaved in a ductile manner and testing proceeded in a smooth and controlled way. It was found that, after the steel reached its yield strain, an outward indent or bulge formed closely to the stub at the compression face of the composite column on both sides of the stub. The bulge also formed on the other face of the specimen when the lateral load was reversed. The bulge then grew with increasing lateral displacement until the bulge formed a complete ring on each side of

(a) Steel tube

(a) Steel tube

(b) Concrete core

(b) Concrete core

(1) Circular column

(2) Square column
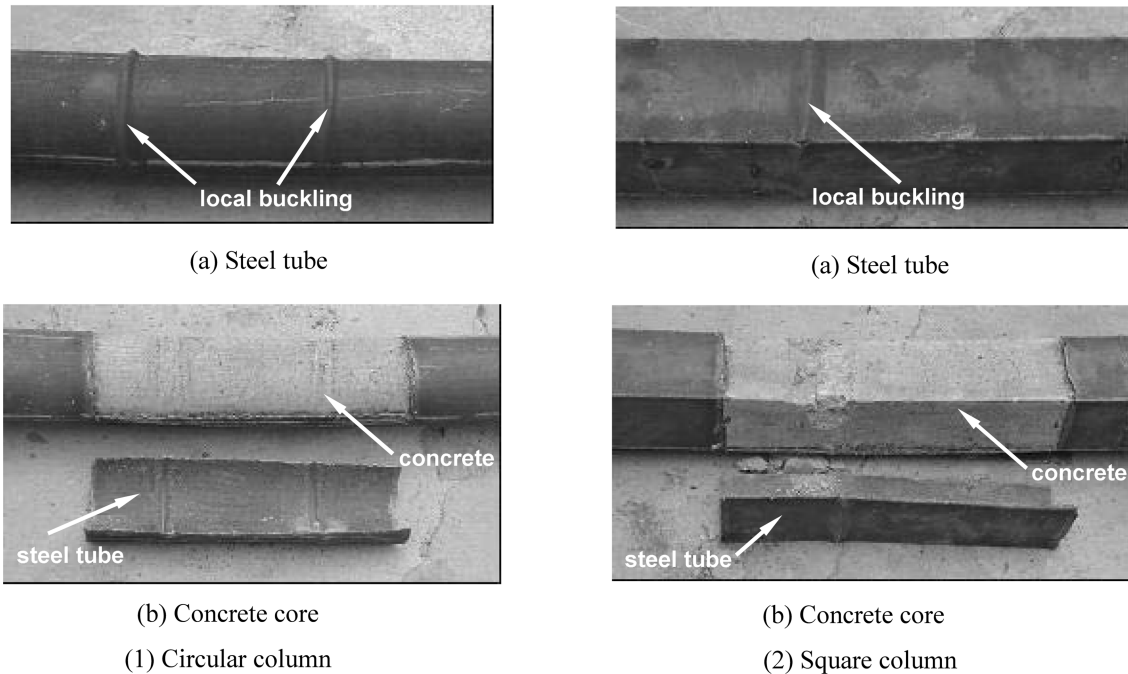
Fig. 14 Typical failure mode of the tested specimens

the stub. All of the tested specimens failed due to tensile fracture at the bulge location, accompanied with a sudden drop in the lateral load bearing capacity. It was found that the failure features of the STCC specimens after cyclic loadings were very similar to those of the CFST columns (Elremaily and Azizinamini 2002, Han *et al.* 2003a, Han and Yang 2005).

Fig. 14 shows typical failure mode of the steel tubes and their concrete core after the test, and removing the middle stub.

The tested curves of lateral load (P) versus the mid-span displacement (Δ) curves for circular and square specimens are shown in Figs. 15 and 16 respectively. The maximum lateral loads (P_{ue}) obtained in the tests are summarized in Table 5.

Specimen CCB-1 (with the axial load level of 0.37) is selected to demonstrate the typical response of the measured moment (M) versus curvature (ϕ) graphs, as shown in Fig. 17. The moment versus curvature diagrams show that there is an initial elastic response, then an inelastic behavior with gradually decreasing stiffness, until the ultimate moment is reached asymptotically. A careful examination of the test results revealed that, in general, the moment versus curvature relationship enters the inelastic stage at 20% of the moment capacity (M_u), so the initial section flexural stiffness (K_i) is defined as the secant stiffness corresponding to the moment of $0.2\,M_u$. The moment versus curvature response is also used to determine the serviceability-level section flexural stiffness (K_S). K_S is defined as the secant stiffness corresponding to the serviceability-level moment of $0.6\,M_u$ (Varma *et al.* 2002). The initial section flexural stiffness (K_{ie}) and the serviceability-level section flexural stiffness (K_{se}) of the tested specimens so determined are listed in Table 5 respectively.
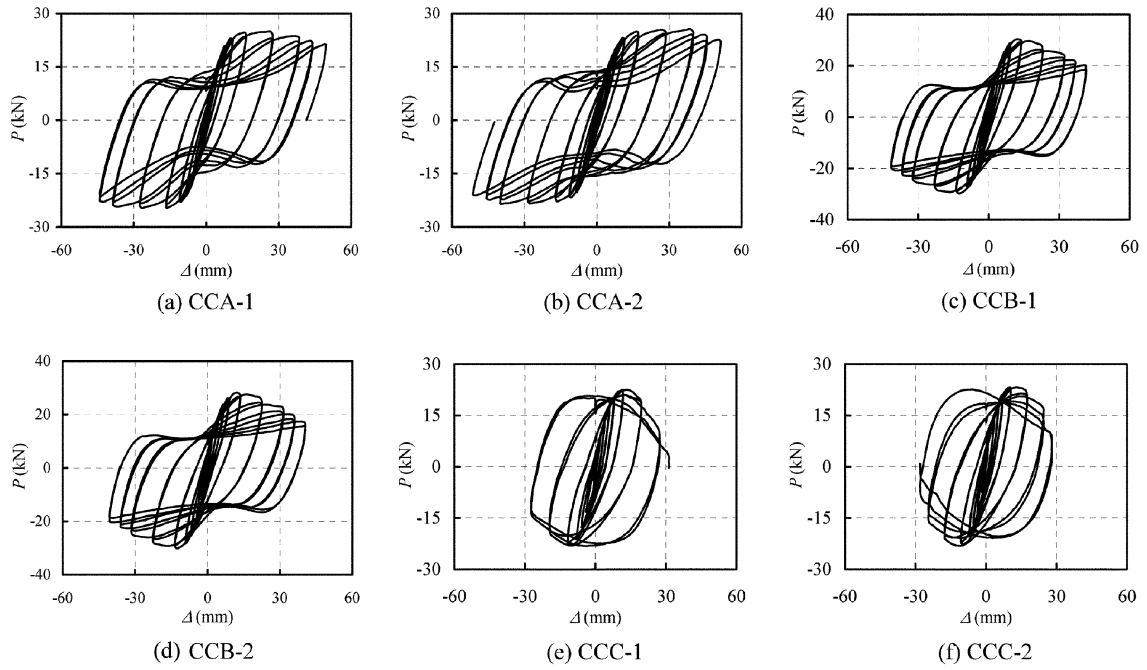
Fig. 15 Cyclic load (P) versus lateral displacement (Δ) for tested specimens (circular sections)
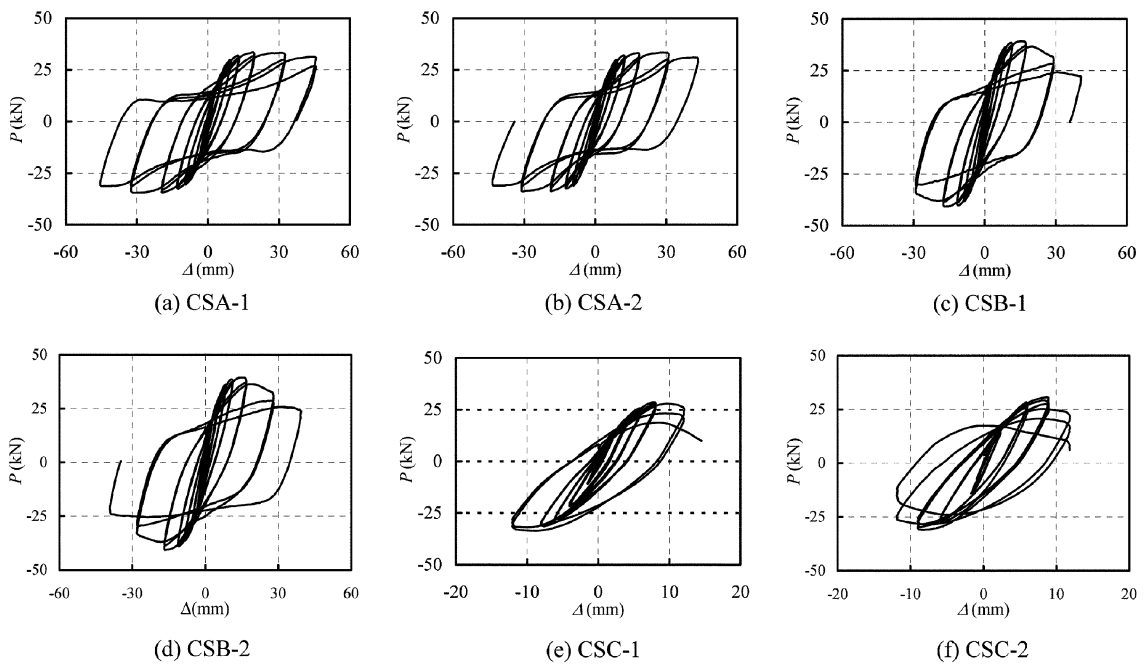
Fig. 16 Cyclic load (P) versus lateral displacement (Δ) for tested specimens (square columns)
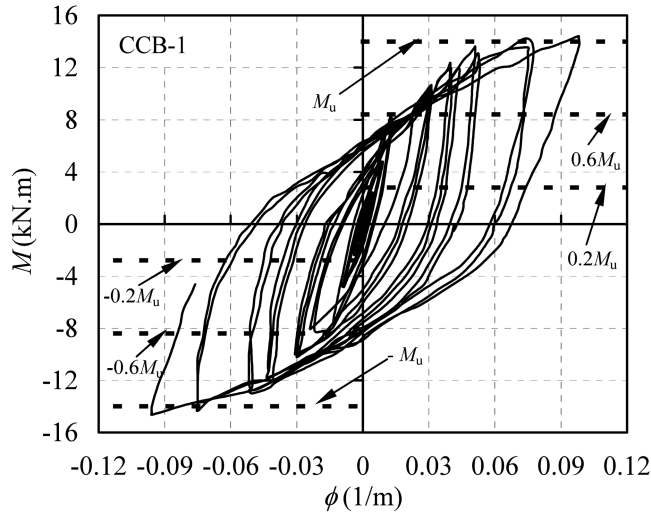
Fig. 17 Typical moment (M) versus curvature (ϕ) relations (CCB-1)

(a) Circular specimens   (b) Square specimens

Fig. 18 Influence of axial load levels on lateral load (P) versus lateral deflection (Δ) envelope curves

4.4. Analysis of test results and discussions

4.4.1. Effects of axial load level

Fig. 18 and Fig. 19 show the influence of axial load levels on the lateral load (P) versus lateral displacement (Δ) envelope curves, as well as the moment (M) versus curvature (ϕ) envelope curves of the tested specimens respectively. It can be found from this figure that, the axial load level (n) influences not only the ultimate lateral load (P_{ue}), but also the ductility of the specimen. Generally, the ductility of the specimen decreases with the increases in the axial load level.

Fig. 20 shows the relationship between lateral strength (P_{ue}) versus axial load level (n), it can be concluded that, in general, the ultimate lateral strength (P_{ue}) increases with the increase in axial load

(a) Circular specimens (b) Square specimens
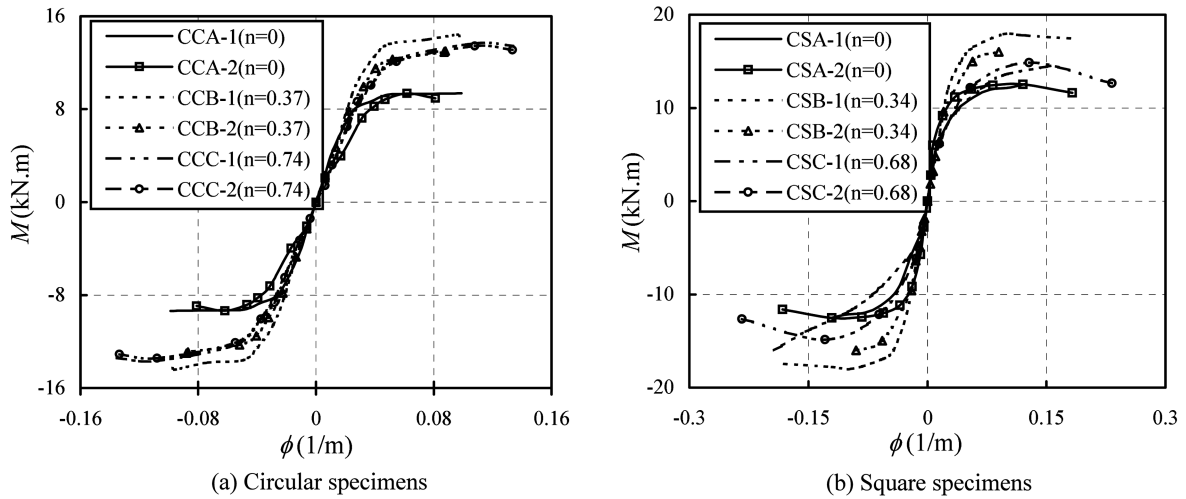
Fig. 19 Influence of axial load levels on moment (M) versus curvature (ϕ) envelope curves

(a) Circular specimens (b) Square specimens
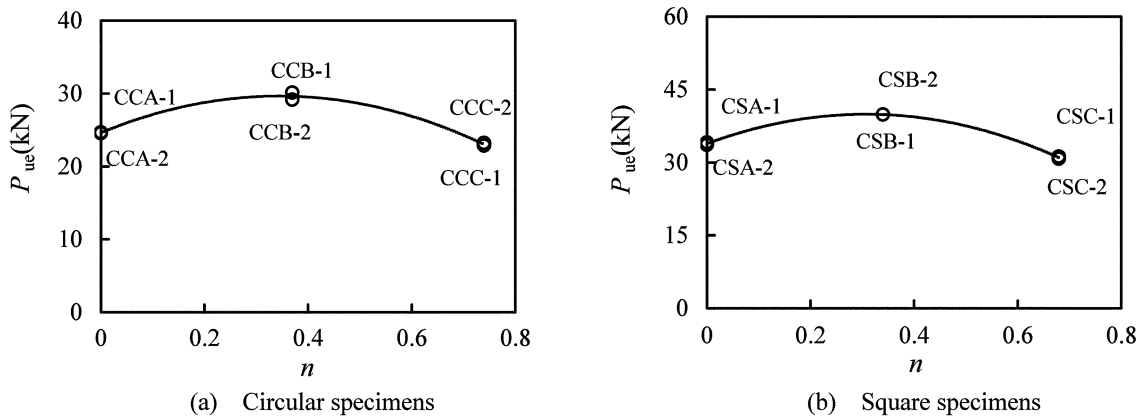
Fig. 20 Relationship between lateral strength (P_{ue}) and axial load level (n)

level (n) when it is smaller (less than 0.35), however, P_{ue} decreases with the increase in axial load level (n) when n is bigger than 0.35 for the current tested specimens.

4.4.2. Dissipated energy, rigidity degradation

Fig. 21 shows that the dissipated energy in each cycle is calculated from the lateral load (P) versus lateral displacement (Δ) curve as the area bound by the hysteretic hoop of that cycle. The values of the total energy dissipated through each test were shown in Table 5. The table indicates that, in general, the dissipated energy ability of specimens with circular sections is higher than those of the specimens with square sections.

Fig. 22 shows the ratio between the column flexural stiffness (K) obtained from the test data and the calculated initial flexural stiffness K_e, in which, K_e is the elastic flexural stiffness of the composite columns listed in BS5400 (1979), i.e.,

(a)   Circular specimens   (b)   Square specimens
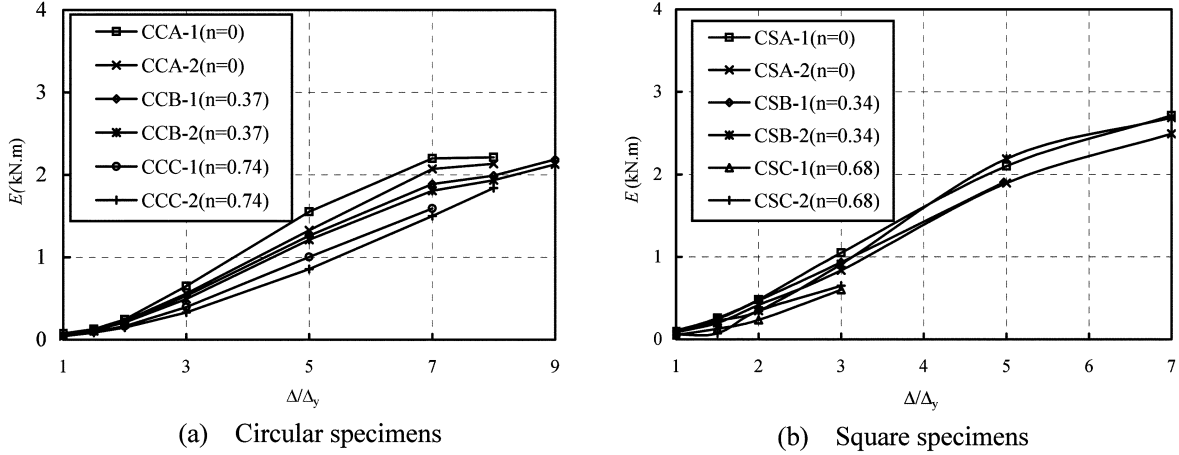
Fig. 21 Energy (E) dissipation ability

(a)   Circular specimens   (b)   Square specimens
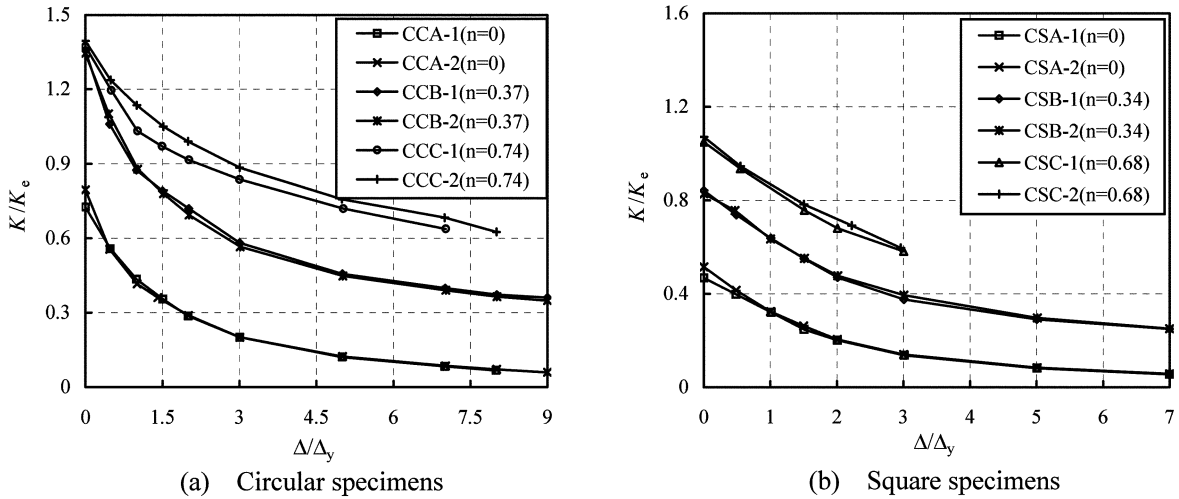
Fig. 22 Rigidity degradation

$$K_e = E_s \cdot I_s + E_c \cdot I_c \tag{4}$$

where $E_S = 206000(\text{MPa})$; $E_c = 450 \cdot f_{cu}(\text{MPa})$ are the elastic modulus of the steel tube and concrete respectively; I_s and I_c are the moment of inertia for the structural steel tube and the gross concrete section respectively.

It was found from Fig. 22 that, for circular STCC specimens, the degradation of the flexural stiffness ranged from 53.6% to 92.5%. And, for the square STCC specimens, the measured degradation of the flexural stiffness ranged from 44.3% to 88.8%.

4.4.3. Comparisons of lateral strength of the composite columns

The ultimate lateral strength (P_u) of the composite columns can be determined by using the following design methods, i.e.,

- AIJ (1997)
- AISC-LRFD (1999)
- BS5400 (1979)
- EC4 (1994)

In all design calculations, the material partial safety factors were set to unity.

It should be noted that the current code provisions were not originally developed for STCC columns under constant axial load and cyclically increasing flexural loading. The purpose of the comparison was to evaluate their accuracy in predicting the capacity of the STCC beam-column specimens.

Comparisons of the tested ultimate lateral load (P_{ue}) with predictions (P_{uc}) based on the code provisions are shown in Table 6.

Table 6 shows both the mean value and the standard deviation (COV) of the ratio of P_{uc}/P_{ue} for the different design methods. Results in this table clearly show that all of the methods are conservative. For columns with circular sections, AISC-LRFD (1999) and BS5400 (1979) gave ultimate lateral strength which is about 57% and 44% lower than that of the test. EC4 (1994) and AIJ (1997) gave ultimate lateral strength which is about 24% and 38% lower than those of the tests respectively. For columns with square sections, AISC-LRFD(1999) and BS5400 (1979) gave ultimate lateral strength which is about 50% and 36% lower than that of test. EC4 (1994) and AIJ (1997) gave ultimate lateral strength which is about 10% and 21% lower than those of the tests respectively. Relatively, the proposed method

Table 6 Comparisons between predicted member capacities and test results(cyclic tests)

Section type	No.	Specimen Number	P_{ue} (kN)	AIJ (1997)		AISC-LRFD (1999)		BS5400 (1979)		EC4(1994)	
				P_{uc} (kN)	$\dfrac{P_{uc}}{P_{ue}}$	P_{uc} (kN)	$\dfrac{P_{uc}}{P_{ue}}$	P_{uc} (kN)	$\dfrac{P_{uc}}{P_{ue}}$	P_{uc} (kN)	$\dfrac{P_{uc}}{P_{ue}}$
Circular	1	CCA-1	24.68	17	0.689	17	0.689	19.6	0.794	21.5	0.871
	2	CCA-2	24.55	17	0.692	17	0.692	19.6	0.798	21.5	0.876
	3	CCB-1	30.1	22.4	0.744	11.9	0.395	16.4	0.545	23.3	0.774
	4	CCB-2	29.15	22.4	0.768	11.9	0.408	16.4	0.563	23.3	0.799
	5	CCC-1	22.85	9.6	0.420	4.7	0.206	7.9	0.346	14.6	0.639
	6	CCC-2	23.2	9.6	0.414	4.7	0.203	7.9	0.341	14.6	0.629
	Mean value			0.621		0.432		0.564		0.765	
	Standard Deviation (COV)			0.161		0.219		0.203		0.109	

Section type	No.	Specimen Number	P_{ue} (kN)	AIJ (1997)		AISC-LRFD (1999)		BS5400 (1979)		EC4(1994)	
				P_{uc} (kN)	$\dfrac{P_{uc}}{P_{ue}}$	P_{uc} (kN)	$\dfrac{P_{uc}}{P_{ue}}$	P_{uc} (kN)	$\dfrac{P_{uc}}{P_{ue}}$	P_{uc} (kN)	$\dfrac{P_{uc}}{P_{ue}}$
Square	1	CSA-1	33.99	25.5	0.748	25.5	0.748	30.7	0.901	31.2	0.915
	2	CSA-2	33.55	25.5	0.759	25.5	0.759	30.7	0.914	31.2	0.929
	3	CSB-1	39.98	36	0.904	19	0.477	25.2	0.633	36.6	0.919
	4	CSB-2	40.05	36	0.903	19	0.477	25.2	0.632	36.6	0.918
	5	CSC-1	31.18	22.1	0.709	9.2	0.295	11.9	0.382	27	0.866
	6	CSC-2	30.78	22.1	0.718	9.2	0.299	11.9	0.387	27	0.877
	Mean value			0.790		0.509		0.641		0.904	
	Standard Deviation (COV)			0.090		0.206		0.234		0.026	

in EC4 (1994) gave a mean value of 0.765 and 0.904, a COV of 0.109 and 0.026 for STCC specimens with circular and square sections respectively, and it is the best means of prediction.

4.4.4. Flexural stiffness

The elastic flexural stiffness (K_e) can be calculated by using Eq. (4) by BS5400 (1979), or the equations listed in the following design standards, i.e.,
(1) AIJ (1997)

$$K_e = E_s \cdot I_s + 0.2 E_c \cdot I_c \tag{5}$$

where $E_s = 205800$ (MPa); $E_c = 21000 \sqrt{f_c' / 19.6}$ (MPa).
(2) AISC-LRFD (1999)
In AISC-LRFD (1999), K_e is given as $K_e = [E_s + 0.4 E_c (A_c / A_s)] \cdot I_s$, and it can be approximately expressed as

$$K_e = E_s \cdot I_s + 0.8 E_c \cdot I_c \tag{6}$$

where $E_s = 200000$ (MPa); $E_c = 4733 \sqrt{f_c'}$ (MPa).
(3) EC 4 (1994)

Table 7 Comparisons between predicted initial section flexural stiffness (K_{ic}) and test results

Section type	No.	Specimen Number	K_{ie} (kN.m²)	AIJ (1997)		AISC-LRFD (1999)		BS5400 (1979)		EC4(1994)	
				K_{ic} (kN.m²)	$\frac{K_{ic}}{K_{ie}}$	K_{ic} (kN.m²)	$\frac{K_{ic}}{K_{ie}}$	K_{ic} (kN.m²)	$\frac{K_{ic}}{K_{ie}}$	K_{ic} (kN.m²)	$\frac{K_{ic}}{K_{ie}}$
Circular	1	CCA-1	358	251	0.701	399	1.115	376	1.050	383	1.070
	2	CCA-2	340	251	0.738	399	1.174	376	1.106	383	1.126
	3	CCB-1	378	251	0.664	399	1.056	376	0.995	383	1.013
	4	CCB-2	370	251	0.678	399	1.078	376	1.016	383	1.035
	5	CCC-1	363	251	0.691	399	1.099	376	1.036	383	1.055
	6	CCC-2	365	251	0.688	399	1.093	376	1.030	383	1.049
	Mean value			0.693		1.102		1.039		1.058	
	Standard Deviation (COV)			0.025		0.040		0.038		0.039	

Section type	No.	Specimen Number	K_{ie} (kN.m²)	AIJ (1997)		AISC-LRFD (1999)		BS5400 (1979)		EC4(1994)	
				K_{ic} (kN.m²)	$\frac{K_{ic}}{K_{ie}}$	K_{ic} (kN.m²)	$\frac{K_{ic}}{K_{ie}}$	K_{ic} (kN.m²)	$\frac{K_{ic}}{K_{ie}}$	K_{ic} (kN.m²)	$\frac{K_{ic}}{K_{ie}}$
Square	1	CSA-1	509	426	0.837	678	1.332	674	1.324	650	1.277
	2	CSA-2	644	426	0.661	678	1.053	674	1.047	650	1.009
	3	CSB-1	534	426	0.798	678	1.270	674	1.262	650	1.217
	4	CSB-2	511	426	0.834	678	1.327	674	1.319	650	1.272
	5	CSC-1	562	426	0.758	678	1.206	674	1.199	650	1.157
	6	CSC-2	514	426	0.829	678	1.319	674	1.311	650	1.265
	Mean value			0.786		1.251		1.244		1.199	
	Standard Deviation (COV)			0.068		0.108		0.108		0.104	

$$K_e = E_s \cdot I_s + 0.6 E_c \cdot I_c \tag{7}$$

where $E_s = 206000$ (MPa); $E_c = 9500 \cdot (f_c' + 8)^{\frac{1}{3}}$ (MPa).

Predicted initial section flexural stiffness (K_{ic}) of the composite columns based on the code provisions for CFST is compared with the current STCC experimental results (K_{ie}) in Table 7.

Table 7 shows both the mean value and the standard deviation (COV) of the ratio K_{ic}/K_{ie} for the different design methods. Results in Table 7 clearly show that, for specimens with circular sections, EC4 (1994) and AISC-LRFD (1999) gave the initial section flexural stiffness about 6% and 10% higher than those of the tests respectively. AIJ (1997) gave the initial section flexural stiffness about 30% lower than that of the test. The BS5400 (1979) method gives a mean of 1.039 and a COV of 0.038 and is the best means of prediction. For columns with square sections, BS5400 (1979), EC4 (1994) and AISC-LRFD (1999) gave the initial section flexural stiffness about 24%, 20% and 25% higher than those of the tests respectively. The AIJ (1997) method gives a mean of 0.786 and a COV of 0.068 and it predicted a lower stiffness than the test results.

Predicted serviceability-level section flexural stiffness (K_{sc}) of the composite columns based on the code provisions for CFST is compared with the current STCC experimental results (K_{se}) in Table 8. Table 8 shows both the mean value and the standard deviation (COV) of the ratio K_{sc}/K_{se} for the

Table 8 Comparisons between predicted serviceability-level section flexural stiffness (K_{sc}) and test results

Section type	No.	Specimen Number	K_{se} (kN.m²)	AIJ (1997)		AISC-LRFD (1999)		BS5400 (1979)		EC4(1994)	
				K_{sc} (kN.m²)	$\dfrac{K_{sc}}{K_{se}}$	K_{sc} (kN.m²)	$\dfrac{K_{sc}}{K_{se}}$	K_{sc} (kN.m²)	$\dfrac{K_{sc}}{K_{se}}$	K_{sc} (kN.m²)	$\dfrac{K_{sc}}{K_{se}}$
Circular	1	CCA-1	343	251	0.732	399	1.163	376	1.096	383	1.117
	2	CCA-2	300	251	0.837	399	1.330	376	1.253	383	1.277
	3	CCB-1	360	251	0.697	399	1.108	376	1.044	383	1.064
	4	CCB-2	349	251	0.719	399	1.143	376	1.077	383	1.097
	5	CCC-1	332	251	0.756	399	1.202	376	1.133	383	1.154
	6	CCC-2	307	251	0.818	399	1.300	376	1.225	383	1.248
	Mean value			0.760		1.208		1.138		1.159	
	Standard Deviation (COV)			0.056		0.089		0.084		0.085	

Section type	No.	Specimen Number	K_{se} (kN.m²)	AIJ (1997)		AISC-LRFD (1999)		BS5400 (1979)		EC4(1994)	
				K_{sc} (kN.m²)	$\dfrac{K_{sc}}{K_{se}}$	K_{sc} (kN.m²)	$\dfrac{K_{sc}}{K_{se}}$	K_{sc} (kN.m²)	$\dfrac{K_{sc}}{K_{se}}$	K_{sc} (kN.m²)	$\dfrac{K_{sc}}{K_{se}}$
Square	1	CSA-1	422	426	1.009	678	1.607	674	1.597	650	1.540
	2	CSA-2	497	426	0.857	678	1.364	674	1.356	650	1.308
	3	CSB-1	464	426	0.918	678	1.461	674	1.453	650	1.401
	4	CSB-2	472	426	0.903	678	1.436	674	1.428	650	1.377
	5	CSC-1	476	426	0.895	678	1.424	674	1.416	650	1.366
	6	CSC-2	438	426	0.973	678	1.548	674	1.539	650	1.484
	Mean value			0.926		1.473		1.465		1.413	
	Standard Deviation (COV)			0.056		0.088		0.088		0.085	

different design methods. Results in this table clearly show that for columns with circular sections, BS5400 (1979), EC4 (1994) and AISC-LRFD (1999) gave the serviceability-level section flexural stiffness about 14%, 16% and 21% higher than those of tests respectively. The AIJ (1997) method gave the mean of 0.760, the COV of 0.056, predicted about 24% lower flexural stiffness than the test results. For specimens with square sections, BS5400 (1979), EC4 (1994) and AISC-LRFD (1999) gave the serviceability-level section flexural stiffness about 46%, 41%, and 47% higher than that of the test respectively. The AIJ (1997) method gave the mean of 0.926, the COV of 0.056, predicted about 7% lower flexural stiffness than the test results, and is the best mean of prediction.

5. Conclusions

The present study is an attempt to study the possibility of using STCC columns in practice. Based on the results of this study, the following conclusions can be drawn within the scope of these tests:
(1) It was found that, in general, the sectional capacity of STCC stub columns is slightly higher than those of the CFST specimens, however, the member capacity of STCC columns is slightly lower, but comparable value to that of the CFST specimens.
(2) For STCC columns under monotonously loading states, it was found that, generally, both AIJ, AISC-LRFD and BS5400 methods for CFST are conservative for predicting the strengths of the STCC specimens. However, EC4 gave a slightly higher bearing capacity than these of the measured ultimate strength.
(3) Steel tube confined concrete (STCC) columns exhibit very high levels of energy dissipation and ductility. Generally, the energy dissipation ability of the columns with circular sections was higher than those of the specimens with square sections.
(4) Comparisons are made with predicted column strengths and flexural stiffness using the existing codes for CFST columns under cyclically loading states, such as AISC-LRFD (1999), AIJ (1997), BS5400 (1979) and EC4 (1994). It was found that, in general, the provisions developed for CFST columns mentioned above underestimate the moment capacity of the STCC members.

Acknowledgements

References

Aboutaha, R.S. and Machado, R. (1998), "Seismic resistance of steel confined reinforced concrete (SCRC) columns", *The Structural Design of Tall Buildings*, **7**(3), 251-260.
Architectural Institute of Japan (AIJ). Recommendations for Design and Construction of Concrete Filled Steel Tubular Structures. Tokyo, Japan, 1997.
AISC (1999), "Load and resistance factor design (LRFD) specification for structural steel buildings", American Institute of Steel Construction, Inc., Chicago.
ASCCS (1997), "Concrete filled steel tubes − A comparison of international codes and practices", ASCCS

Seminar Report, Innsbruck.

ATC-24 (1992), "Guidelines for cyclic seismic testing of components of steel structures", Redwood City (CA): Applied Technology Council.

British Standard Institute (1979), "BS5400, Part 5, Concrete and composite bridges", London, UK.

Elremaily, A. and Azizinamini, A. (2002), "Behavior and strength of circular concrete-filled tube columns", *J. Constructional Steel Research*, **58**(12), 1567-1591.

Eurocode 4 (1994), "Design of composite steel and concrete structures, Part1.1: General rules and rules for buildings (together with united kingdom national application document)", DD ENV 1994-1-1:1994, British Standards Institution, London W1A2BS.

Fam, A., Qie, F.S. and Rizkalla, S. (2004), "Concrete-filled steel tubes subjected to axial compression and lateral cyclic loads", *J. Struct. Eng.*, ASCE, **130**(4), 631-640.

Han, L.H. and Yang, Y.F. (2005), "Cyclic performance of concrete-filled steel CHS columns under flexural loading", *J. Constructional Steel Research*, **61**(4), 423-452.

Han, L.H., Yang, Y.F. and Tao, Z. (2003a), "Concrete-filled thin walled steel RHS beam-columns subjected to cyclic loading", *Thin-walled Structures*, **41**(9), 801-833.

Han, L.H. and Yao, G.H. (2004), "Experimental behaviour of thin-walled hollow structural steel (HSS) columns filled with self-consolidating concrete (SCC)", *Thin Walled Structures*, **42**(9), 1357-1377.

Han, L.H., Yao, G.H. and Zhao, X.L. (2004), "Behavior and calculation on concrete-filled steel CHS (circular hollow section) beam-columns", *Steel and Composite Structures, An Int. J.*, **4**(3), 787-804.

Han, L.H., Zhao, X.L. and Tao, Z. (2001), "Tests and mechanics model for concrete-filled shs stub columns, columns and beam-columns", *Steel and Composite Struct. An Int. J.*, **1**(1), 51-74.

Han, L.H., Zhao, X.L., Yang, Y.F. and Feng, J.B. (2003b), "Experimental study and calculation of fire resistance of concrete-filled hollow steel columns", *J. Struct. Eng.*, ASCE, **129**(3), 346-356.

Johansson, M. (2002), "The efficiency of passive confinement in CFT columns", *Steel and Composite Structures, An Int. J.*, **2**(5), 379-396.

Orito, Y., Sato, Y., Tanaka, N., and Watanabe, Y. (1987), "Study on the unbonded steel tube concrete structure", *Engineering Foundation Conf. on Composite Constructions*, Henniker, New Hampshire, USA, 786-804.

O'Shea, M.D. and Bridge, R.Q. (1997a), "Tests on circular thin-walled steel tubes filled with medium and high strength concrete", Department of Civil Engineering Research Report No. R755, the University of Sydney, Sydney, Australia.

O'Shea, M.D. and Bridge, R.Q. (1997b), "Tests on circular thin-walled steel tubes filled with very high strength concrete", Department of Civil Engineering Research Report No. R754, the University of Sydney, Sydney, Australia.

Sakino, K., Tomii, M. and Watanabe, K. (1985), "Sustaining load capacity of plain concrete stub columns confined by circular steel tubes", *Proc. of the Int. Specialty Conf. on Concrete-Filled Steel Tubular Structures*, ASCCS, Harbin, China, 112-118.

Schneider, S.P. (1998), "Axially loaded concrete-filled steel tubes", *J. Struct. Eng.*, ASCE, **124**(10), 1125-1138.

Schneider, S.P., Kramer, D.R. and Sarkkinen, D.L.(2004), "The design and construction of concrete-filled steel tube column frames", *Proc. of the 13th World Conf. on Earthquake Engineering* (Paper No. 252), Vancouver, B.C., Canada, August 1-6.

Varma A.H., Ricles, J.M., Sause, R. and Lu, L.W. (2002), "Seismic behavior and modeling of high-strength composite concrete-filled steel tube (CFT) beam-columns", *J. Constructional Steel Research*, **58**(5-8), 725-758.

Notation

A_s	: Steel cross-sectional area
A_c	: Concrete cross-sectional area
CFST	: Concrete filled steel tubes
D	: Sectional dimension, in mm
D/t	: Tube diameter (or width) to thickness ratio
e	: Eccentricity of load, in mm
e/r	: Load eccentricity ratio, $r = D/2$
E_c	: Concrete modulus of elasticity
E_s	: Steel modulus of elasticity
f_{sy}	: Yield strength of steel
f_{cu}	: Concrete cube strength
f_c'	: Concrete cylinder strength
I_s	: Moment of inertia of the steel tube
I_c	: Moment of inertia of the concrete section
K_i	: Initial section flexural stiffness of the composite column
K_S	: Serviceability-level section flexural stiffness of the composite column
L	: Effective buckling length of column in the plane of bending
M	: Moment
M_u	: Moment capacity
n	: Axial load level ($= N_o / N_u$)
N_o	: Axially compressive load
N_u	: Ultimate strength of the composite columns
N_{uc}	: Predicted ultimate strength
N_{ue}	: Experimental ultimate strength
u_m	: Mid-height deflection of the column, in mm
P_u	: Ultimate lateral strength of the composite columns
P	: Lateral load
P_{uc}	: Predicted lateral strength
P_{ue}	: Experimental lateral strength
SCC	: Self-consolidating concrete
STCC	: Steel tube confined concrete
t	: Wall thickness of steel tube, in mm
ϕ	: Curvature
Δ	: Lateral displacement
ε	: Strain
λ	: Slenderness ratio, given by $4L/D$ and $2\sqrt{3}L/D$ for column with circular section and square section respectively
CC	